



OPEN

DATA DESCRIPTOR

3D meshes dataset of sagittal otoliths from red mullet in the Mediterranean Sea

Nicolas Andrialovanirina^{1,2}  , Lauriane Poloni^{3,4}, Rémi Laffont⁴, Émilie Poisson Caillault¹, Sébastien Couette^{3,4} & Kélig Mahé²  

This paper presents a dataset of 3D sagittal left otolith meshes from 339 individual red mullet (*Mullus barbatus*). These immature specimens were collected from 17 geographical areas covering the entire Mediterranean Sea. Measured biological parameters were: fish total length (TL \pm 1 mm, range from 125 to 238 mm), total weight (W \pm 0.1 g, range from 14.9 to 168.0 g), sex (S), sexual maturity staging (Mat). The 3D otolith dataset comprises high-resolution meshes of otoliths obtained using microtomography (29.2 μ m voxel size). The data offer valuable insights into the morphological variability and population structure of red mullet populations in the Mediterranean Sea. Potential applications of the dataset include age determination, stock identification, and population connectivity analysis. These applications aim to enhance the understanding of red mullet populations and contribute to the sustainable management of marine resources in the Mediterranean Sea.


Background & Summary

Among the numerous fish species inhabiting the Mediterranean Sea, the red mullet (*Mullus barbatus*) stands out as a primary commercial species supporting artisanal and industrial fisheries across this geographical area¹. Understanding the dynamics and structure of red mullet populations is essential for sustainable fisheries management in the Mediterranean. The otolith contains valuable clues about the life history of individual fish and the environmental pressures they experience^{2–5}.

The otolith, a incrementally grown calcified structure located in the inner-ear of fishes, plays a crucial role in hearing, balance and orientation⁶. It is found within otic sacs in a network of semicircular canals inside the ear. These otic sacs contain three pairs of otoliths known as *sagitta*, *lapillus*, and *lagena*⁷. The data presented in this paper pertains only to the sagittal otolith, which is generally the most voluminous and the most commonly studied in fisheries applications^{2,4,5}. Otolith shape is influenced by a multifaceted interaction among environmental factors^{8–18}, genetic inheritance^{11,14,16}, and ontogenetic development^{12,19–21}. Otoliths are metabolically inert (*i.e.*, without post-deposition alteration or resorption)⁶, and their extraction and processing are less time-consuming and less expensive than other methods of stock delimitation (*e.g.*, genetics)². Therefore, it has become one of the most widely used proxies for age estimation, identifying stock boundaries, and population connectivity analysis of various fish species^{2,5}.

Traditionally, otolith shape analysis has been conducted using two-dimensional (2D) images⁵, which offer only a limited perspective of the three-dimensional (3D) structure. This approach may introduce biases due to the object's positioning during 2D image acquisition. Recent advancements in imaging technology have enabled the application of 3D shape analysis to otoliths, providing a more comprehensive understanding of their morphology. By capturing the whole 3D surface of otoliths in three dimensions, this method offers deeper insights into their structural complexity and biological significance.

3D analysis reveals features that are often overlooked in 2D analysis, thereby expanding our knowledge of otolith morphology. However, research on 3D otoliths has primarily focused on acquisition methods^{22–26} and understanding their function within the fish inner-ear^{27–30}, rather than on aspects applied to shape analysis. A recent study using part of the present dataset from red mullet otoliths demonstrated the effectiveness of 3D

¹Univ. Littoral Côte d'Opale, UR 4491, LISIC, Calais, F-62100, France. ²Ifremer, Unité HMMN, Laboratoires Ressources Halieutiques, 150 quai Gambetta, Boulogne-sur-Mer, 62321, France. ³École Pratique des Hautes Études, PSL Université, Paris, 75014, France. ⁴UMR CNRS 6282 Biogéosciences, Université de Bourgogne, 6 Bd Gabriel, Dijon, 21000, France. e-mail: nicolas.andrialovanirina@ifremer.fr; kelig.mahe@ifremer.fr

n° GSA	1	5	6	8	10	11	12	14	16	17	18	20	22	23	24	25	27
n samples	7	23	12	12	13	5	19	16	58	8	30	20	36	19	22	24	27

Table 1. Sampling distribution by geographical sub-areas (GSAs).

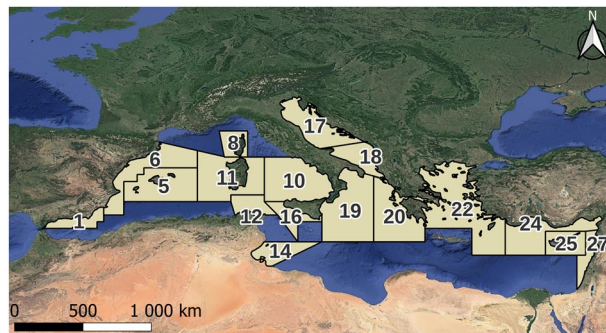


Fig. 1 Location of fish sampling from 17 geographical sub-areas (GSAs) in the Mediterranean Sea.

analysis in addressing significant asymmetry originating from the inner-ear side, a phenomenon not observed in 2D analysis with the same otoliths³¹. Additionally, this 3D asymmetry also influenced the fish's location, *i.e.* the intensity of the asymmetry varied depending on the fish's environment. Consequently, this dataset on the 3D shape of fish otoliths represents a new opportunity for better understanding their morphogenesis processes. With the 3D meshes data, research could delve deeper into the relationship with fish growth (*i.e.* ontogeny evolution), genetic heritage, and the environmental parameters of the habitat, allowing for a more comprehensive exploration and understanding their impact of these factors on the otolith.

This paper presents a comprehensive dataset of 3D sagittal otolith meshes of red mullet collected from 17 locations from the Mediterranean Sea. The dataset includes high-resolution images obtained using micro-computed tomography (micro-CT or μ CT). Each otolith image is available with the individual biological parameters of each specimen. These measurements provide valuable information on the shape variability of red mullet otoliths, which can be used to infer age, assess growth rates, and identify stock structure. The creation of this dataset was motivated by the need for standardised, high-quality data to support research in fisheries science, marine ecology, and conservation biology. By providing researchers with access to a collection of 3D otolith models and associated biological fish data, this dataset facilitates studies on the population dynamics, connectivity, and resilience of red mullet populations in the Mediterranean Sea. Furthermore, the dataset has the potential for broader applications beyond red mullet research, serving as a valuable resource for comparative studies on otolith morphology and fish population dynamics across different species and geographic regions.

Overall, this dataset represents a valuable resource for researchers interested in studying the ecology, biology, and fisheries management of red mullet populations in the Mediterranean Sea. By facilitating access to 3D otolith data, this dataset contributes to the advancement of scientific knowledge and the development of evidence-based management strategies for sustainable fisheries in the region.

Methods

Fish sampling. 339 individual fish specimens were collected from 17 geographical sub-areas (GSAs) (see Table 1 and Fig. 1), as defined by the General Fisheries Commission for the Mediterranean (GFCM). These GSAs represent diverse fisheries management unit within the Mediterranean Sea. The sampling campaign was conducted during the 2019 international MEDiterranean International Trawl Survey (MEDITS survey), a substantial effort to assess fish populations and their habitats in the Mediterranean Sea³². The MEDITS survey provides a valuable dataset for understanding the distribution and characteristics of fish species.

To ensure robustness in analyse, potential ontogenetic effects on otolith shape are considered. Consequently, the sampling is restricted to young mature fishes (*i.e.* fish after their first sexual maturity and aged between 3 and 5 years old) within a total length range from 125 to 238 mm (with a mean length of 159 ± 19 mm), and a total weight range from 14.9 to 168.0 g (with a mean weight of 46 ± 19 g). Biological fish parameters and sample information were acquired (see Table 2). Furthermore, only left otoliths (*sagittae*) are selected to avoid asymmetric variation. These choices ensure uniformity in our dataset and facilitate accurate comparisons across individuals. Otoliths were carefully extracted from the inner ears of the fish, and cleaned to remove any adhering tissue or debris. Metadata describing the geographic sampling location, and the specimen characteristics (fish total length, weight, sex, maturity stage) were also obtained.

Three-dimensional otolith reconstruction. *X-ray images acquisition.* Otolith X-ray images were acquired using an X-ray microtomograph (micro-CT or μ CT) Skyscan 1174 (Bruker) (see Fig. 2). X-ray microtomography consists on entailed capturing two-dimensional (radiograph) images of the otoliths from various angles, covering a complete rotation from 0° to 180°. The differential attenuation of X-rays while crossing the sample depending of material density, and expressed as different grey values, enable us to discern quite easily the whole otolith from the surrounding air. X-ray microtomograph parameters are showed in Table 3.

Parameters	Detail
Number	Sample identification number
Refscan	Unique sample reference
Species	Latin name of fish species
Meshes3D	3D meshes file name
Sdate	Fish catch date sampling (yyyy-mm-dd)
GSA	Fisheries management unit
Subarea	Geographical sub-area
Latitude	Latitude of the fish sample (in decimal degrees)
Longitude	Longitude of the fish sample (in decimal degrees)
Depth	Estimated depth of catch (in m)
BTemp	Bottom temperature (in celsius degrees)
TL	Total length of the fish, from the tip of the snout to the tip of the longest lobe of the caudal fin (in mm)
W	Total weight of the fish (in g)
S	Sex of the fish (M: male, F: female or I: undetermined)
Mat	Fish sexual maturity staging (0: abnormal <i>i.e.</i> necrotic, sclerotized or intersex gonads; 1: immature; 2: developing gonads, non-hydrated eggs; 3: spawning; 4: regressing or regenerating gonads; 5: no spawning)

Table 2. Sampling details and biological fish parameters.

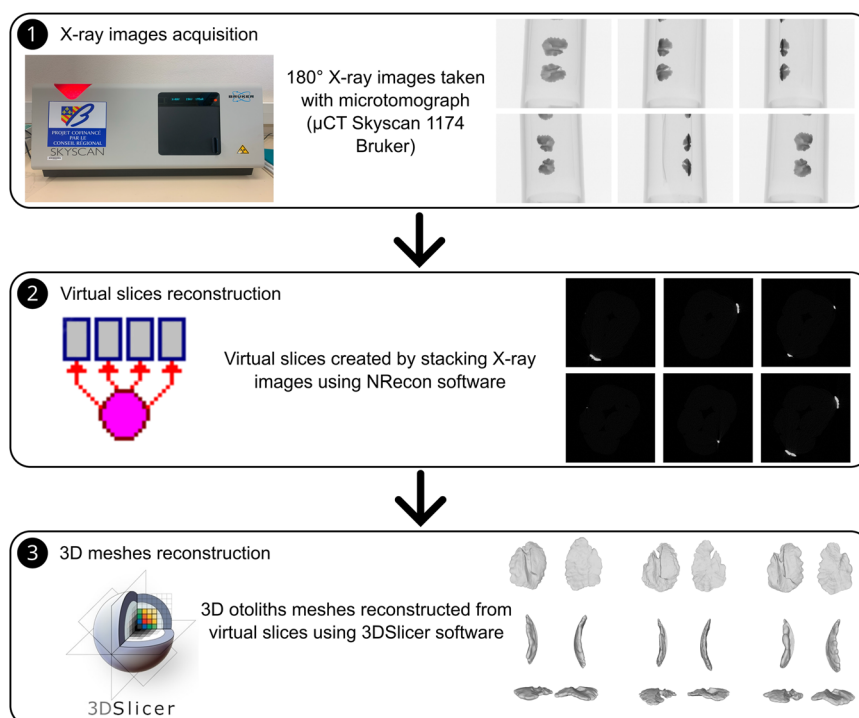


Fig. 2 Method from X-ray images acquisition to 3D otolith meshes.

Virtual slices reconstruction. The software NRecon by Bruker (v.1.7.4.6) was used to reconstruct cross-sectional slices of the otoliths from the radiographs acquired by the microtomograph (see Fig. 2). The program employs a Feldkamp algorithm, a convolution formula, and backprojection to reconstruct a three-dimensional density function from a set of two-dimensional projections. Indeed, X-ray images obtained by microtomography represent grayscale equivalences of material densities (higher densities will be encoded by higher grayscale levels, tending towards white). The algorithm compiles this set of images into a density volume and then generates slices in the transverse plane of this volume at regular intervals. This reconstruction step is automated and also allows for parameter optimization such as volume alignment, artifact correction, or selection of areas of interest. The slice images are saved in Tag Image File Format (.tiff).

3D meshes reconstruction. The segmentation step of the virtual slices aims to distinguish, within the resulting 3D volume of these slices, areas of interest corresponding to the objects under study (see Fig. 2). In this case, the goal is to differentiate between the voxels corresponding to the otoliths and the background voxels based on

Parameters	Measures
Type of scanning	Oversize scan
Rotation step	by 0.7° (from 0° to 180°)
Number of catches	2
Exposure	3,000 ms
Filter	0.5 mm AL
Intensity	800 A
Tube voltage (tension)	50 kV
Voxel size	29.2 μm

Table 3. X-ray microtomograph parameters.

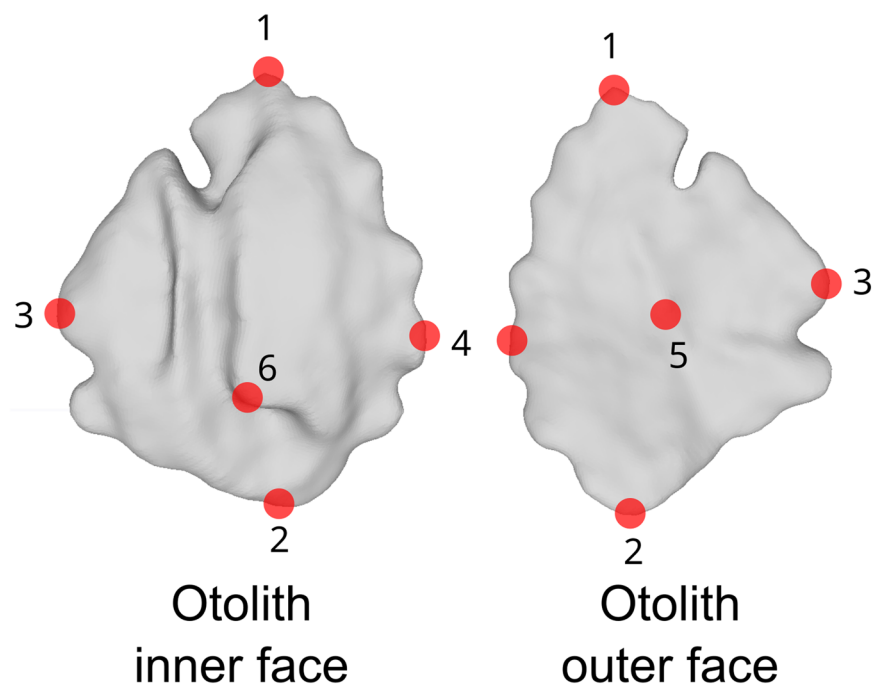


Fig. 3 3D otolith meshes in inner and outer face with six landmarks (red points: 1 at the tip of the *rostrum*, 2 on the *postrostrum*, 3 at the end of dorsal, 4 at the tip of ventral, 5 on the middle of the outer face of the otolith, 6 in the transition part between *ostium* and *cauda*).

simple criteria of grayscale levels (the otolith being dense compared to the background, its constituent voxels will be bright) and adjacency (the otolith constituting a continuous object). This segmentation step is performed using the software 3DSlicer (v.5.0.2). Segmentation Editor module was used with threshold option. Threshold range was between 60 and 255. A grayscale voxel thresholding is applied to select all the voxels constituting the otoliths. The surface of this selected voxel set is then extracted in the form of a 3D mesh (see Fig. 2). This type of object models a 3D mesh as a cloud of points (vertices) connected by triangulation (see Fig. 2) expressing the surface of the 3D segmented object. 3D Slicer uses a Flying edges algorithm for the surface extraction and meshing. Landmarks were manually placed on the meshes to improve the alignment and measurement of the otoliths for future study. We proposed six landmarks (Fig. 3) placed on the meshes using the R package Digit3DLand³³. These landmarks were chosen for their anatomical relevance and ease of identification across specimens, located at the anterior, posterior, dorsal, and ventral edges, as well as the core and a notable curvature point. These landmarks are only subjective, and we strongly recommend automatic alignment. These proposed landmarks could be used for pre-alignment before automatic alignment.

Data Records

3D mesh data was saved in binary Polygon File Format (.ply). The x, y, and z coordinates of six landmarks (refer to Fig. 3) were stored in a TPS text file, where the ID corresponds to the mesh name. Sampling and biological fish parameters were registered in a single comma-separated value (.csv) file. In this csv data, each row corresponds to one fish, with 15 columns as detailed in Table 2. Log file after X-ray images acquisition (.log) and virtual slices reconstruction (_rec.log) were made available. In this way, all the information relating to image acquisition and reconstruction of the virtual slices was saved in these files if necessary. Readme text file is provided for information on the dataset.

All 3D meshes, tps file with landmarks, sampling and biological fish parameters on csv are available on SEANOE (<https://doi.org/10.17882/99980>)³⁴.

Technical Validation

Most shape analysis tools, such as Fourier descriptors, generally require closed objects for processing 3D mesh data. The presence of holes in a 3D object prevents its contour from being analysed.

To address this issue, meshes with holes, non-manifolds (*i.e.*, detached or split edges or vertices) or isolated elements (non otolith artefacts) needed to be identified. To identify 3D meshes with non-manifolds, MeshLab 2022.02 was used. In the following equation (1), genus in mathematic function with Euler characteristic³⁵ were employed to identify manifold meshes with holes.

$$g = -1 \times (0.5 \times (V - E + F + b) - 1) \quad (1)$$

Where g is the genus (number of holes), V is the number of vertices, E is the number of edges, F is the number of faces and b is the number of borders of the 3D meshes.

Subsequently, meshes with holes were either removed or reconstructed by readjusting the threshold range on 3DSlicer. Functions from Rvcg package³⁶ were used to remove isolated artefacts.

Usage Notes

The data³⁴ provided in this paper offer valuable insights into the 3D shape of fish otoliths and can be utilized by researchers across various fields. It is advisable to normalise the data to ensure consistency across different datasets. Researchers may also consider performing additional processing steps, such as alignment, scaling, or feature extraction, depending on their specific research objectives. Landmarks could be used for these purposes. An R script could be supplied to standardise the 3D meshes with the landmarks (decimation, alignment, scale) and then to extract the Fourier coefficients using SPHARM-spherical harmonics³⁷. In SPHARM analysis, landmarks can be used to ensure that the polarity “up-down”, “right-left”, and “front-back” is homologous among the meshes being compared.

Code availability

Pre-processing code was written in R to delete non otolith artefacts, select meshes without holes, save the mesh as a .ply file, and place 6 landmarks for all 3D otolith meshes. The code is available in the supplementary information of this paper.

Received: 21 May 2024; Accepted: 11 July 2024;

Published online: 23 July 2024

References

- Conides, A. & Papaconstantinou, C. Commercial fisheries in the mediterranean, focusing on the environmental status and the corresponding management measures. *Aquaculture and Fisheries Studies* **2**, <https://doi.org/10.31038/AFS.2020214> (2020).
- Cadrin, S., Kerr, L. & Mariani, S. Stock Identification Methods: Applications in Fishery Science (Second Edition). Elsevier Academic Press, Amsterdam (2014).
- Irgens, C. Otolith structure as indicator of key life history events in Atlantic cod (*Gadus morhua*). Ph.D. Thesis, University of Bergen, Norway (2018).
- Mahé, K. Sources de variation de la forme des otolithes : Implications pour la discrimination des stocks de poissons. Ph.D. Thesis, Université du Littoral Côte d'Opale, France <https://doi.org/10.17895/ices.pub.24466996> (2019).
- ICES. ICES stock identification methods working group (SIMWG) **5**, 153, <https://doi.org/10.17895/ices.pub.24466996> (2023).
- Casselman, J. M. Determination of age and growth, In: Weatherley, A. H., Gill, H. S. (Eds.), *The Biology of Fish Growth*. Academic Press, New York (1987).
- Schulz-Mirbach, T., Heß, M., Metscher, B. D. & Ladich, F. A unique swim bladder-inner ear connection in a teleost fish revealed by a combined high-resolution microtomographic and three-dimensional histological study. *BMC Biology* **11**, 75, <https://doi.org/10.1186/1741-7007-11-75> (2013).
- Wilson, R. R. Depth-related changes in sagitta morphology in six macrourid fishes of the pacific and atlantic oceans. *Copeia* **1985**, 1011–1017, <https://doi.org/10.2307/1445256> (1985).
- Morales-Nin, B. Y. O. The influence of environmental factors on microstructure of otoliths of three demersal fish species caught off namibia. *South African Journal of Marine Science* **5**, 255–262, <https://doi.org/10.2989/025776187784522207> (1987).
- Mosegaard, H., Svedäng, H. & Taberman, K. Uncoupling of somatic and otolith growth rates in arctic char (*Salvelinus alpinus*) as an effect of differences in temperature response. *Canadian Journal of Fisheries and Aquatic Sciences* **45**, 1514–1524, <https://doi.org/10.1139/f88-180> (1988).
- Campana, S. E. & Casselman, J. M. Stock discrimination using otolith shape analysis. *Canadian Journal of Fisheries and Aquatic Sciences* **50**, 1062–1083, <https://doi.org/10.1139/f93-123> (1993).
- Lombarte, A. & Lleonart, J. Otolith size changes related with body growth, habitat depth and temperature. *Environmental Biology of Fishes* **37**, 297–306, <https://doi.org/10.1007/BF00004637> (1993).
- Begg, G., Overholtz, W. & Munroe, N. The use of internal otolith morphometrics for identification of haddock (*Melanogrammus aeglefinus*) stocks on georges bank. *Fishery Bulletin* **99** (2001).
- Lombarte, A., Torres, G. J. & Morales-Nin, B. Specific merluccius otolith growth patterns related to phylogenetics and environmental factors. *Journal of the Marine Biological Association of the United Kingdom* **83**, 277–281, <https://doi.org/10.1017/S0025315403007070h> (2003).
- Cardinale, M., Doering-Arjes, P., Kastowsky, M. & Mosegaard, H. Effects of sex, stock, and environment on the shape of known-age atlantic cod (*Gadus morhua*) otoliths. *Canadian Journal of Fisheries and Aquatic Sciences* **61**, 158–167, <https://doi.org/10.1139/f03-151> (2004).
- Vignon, M. & Morat, F. Environmental and genetic determinant of otolith shape revealed by a non-indigenous tropical fish. *Marine Ecology Progress Series* **411**, 231–241, <https://doi.org/10.3354/meps08651> (2010).
- Lewis, L. S. *et al.* Otolith-based approaches indicate strong effects of environmental variation on growth of a critically endangered estuarine fish. *Marine Ecology Progress Series* **676**, 37–56, <https://doi.org/10.3354/meps13848> (2021).

18. Iranmanesh, M., Hesni, M. A. & Lashkari, M. Morphological surveys of the sagittal otolith of marine gobiid fish (teleostei: Gobioidae). *Animal Biology* **73**, 273–291, <https://doi.org/10.1163/15707563-bja10110> (2023).
19. Secor, D. H. & Dean, J. M. Somatic growth effects on the otolith-fish size relationship in young pond-reared striped bass, *Morone saxatilis*. *Canadian Journal of Fisheries and Aquatic Sciences* **46**, 113–121, <https://doi.org/10.1139/f89-015> (1989).
20. Simoneau, M., Casselman, J. M. & Fortin, R. Determining the effect of negative allometry (length/height relationship) on variation in otolith shape in lake trout (*Salvelinus namaycush*), using fourier-series analysis. *Canadian Journal of Zoology* **78**, 1597–1603, <https://doi.org/10.1139/z00-093> (2000).
21. Monteiro, L. R., Benedetto, A. P. M. D., Guillermo, L. H. & Rivera, L. A. Allometric changes and shape differentiation of sagitta otoliths in sciaenid fishes. *Fisheries Research* **74**, 288–299, <https://doi.org/10.1016/j.fishres.2005.03.002> (2005).
22. Zitek, A., Mayrhofer, B., Oehm, J., Irrgeher, J. & Prohaska, T. Affordable 3d scanning of small otoliths for improved shape analysis by photogrammetry techniques <https://doi.org/10.13140/2.1.4083.7122> (2014).
23. Mapp, J. J. I. *et al.* Three-dimensional rendering of otolith growth using phase contrast synchrotron tomography. *Journal of Fish Biology* **88**, 2075–2080, <https://doi.org/10.1111/jfb.12949> (2016).
24. Marti-Puig, P., Danés, J., Manjabacas, A. & Lombarte, A. New parameterisation method for three-dimensional otolith surface images. *Marine and Freshwater Research* **67**, 1059, <https://doi.org/10.1071/MF15069> (2016).
25. Vasconcelos-Filho, J. *et al.* Peeling the otolith of fish: Optimal parameterization for micro-CT scanning. *Frontiers in Marine Science* **6**, <https://doi.org/10.3389/fmars.2019.00728> (2019).
26. Quindazzi, M. J., Summers, A. & Juanes, F. Efficiency is doing things right: high-throughput, automated, 3d methods in the modern era of otolith morphometrics. *Canadian Journal of Fisheries and Aquatic Sciences* **79**, 7, <https://doi.org/10.1139/cjfas-2021-0088> (2022).
27. Schulz-Mirbach, T. *et al.* In-situ visualization of sound-induced otolith motion using hard x-ray phase contrast imaging. *Scientific Reports* **8**, 3121, <https://doi.org/10.1038/s41598-018-21367-0> (2018).
28. Schulz-Mirbach, T., Ladich, F., Plath, M. & Heß, M. Enigmatic ear stones: what we know about the functional role and evolution of fish otoliths. *Biological Reviews* **94**, 457–482, <https://doi.org/10.1111/brv.12463> (2019).
29. Schulz-Mirbach, T. *et al.* Auditory chain reaction: Effects of sound pressure and particle motion on auditory structures in fishes. *PLoS ONE* **15**, e0230578, <https://doi.org/10.1371/journal.pone.0230578> (2020).
30. Wei, C. & McCauley, R. Numerical modeling of the impacts of acoustic stimulus on fish otoliths from two directions. *The Journal of the Acoustical Society of America* **152**, 3226–3234, <https://doi.org/10.1121/10.0016359> (2022).
31. Andrialovanirina, N. *et al.* Asymmetry of sagittal otolith shape based on inner ear side tested on mediterranean red mullet (*Mullus barbatus* linnaeus, 1758): Comparative analysis of 2d and 3d otolith shape data. *Symmetry* **15**, 1067, <https://doi.org/10.3390/sym15051067> (2023).
32. Spedicato, M. T. *et al.* Spatial distribution of marine macro-litter on the seafloor in the northern mediterranean sea: the MEDITS initiative. *Scientia Marina* **83**, <https://doi.org/10.3989/scimar.04987.14A> (2019).
33. Laffont, R. & Navarro, N. digit3dland: Digitalization of 3d landmarks on mesh. *R package version 0.2.3* <https://github.com/morphOptics/digit3Dland>.
34. Andrialovanirina, N. *et al.* 3d otolith mesh dataset of red mullet (*Mullus barbatus*) in the mediterranean sea. *SEANOE* <https://doi.org/10.17882/99980> (2024).
35. Euler, L. Elements of rubrics for solids. *Novi Commentarii Academiae Scientiarum Petropolitanae (in Latin)* 109–140 (1758).
36. Schlager, S. Chapter 9 - morpho and rvcg - shape analysis in r: R-packages for geometric morphometrics, shape analysis and surface manipulations 217–256, <https://doi.org/10.1016/B978-0-12-810493-4.00011-0> (2017).
37. Shen, L., Farid, H. & McPeck, M. A. Modeling three-dimensional morphological structures using spherical harmonics. *Evolution* **63**, 1003–1016, <https://doi.org/10.1111/j.1558-5646.2008.00557.x> (2009).

Acknowledgements

This work has benefited from the grant “ANR-21-EXES-00 11” as part of the IFSEA graduate school (which originates from National Research Agency under the Investments for the Future program), the French Federative Research Structure (SFR Campus de la mer, project No. 2022.7). The otoliths come from the Specific Contract No. 03_EASME/EMFF/2017/1.3.2.3/01/SI2.793201 (MED_UNITS) financed by the European Union. This work is also a contribution to the e-Col+ project funded by the Programme d’Investissements d’Avenir (ANR 21 ESRE 0053). The GISMO platform (Biogéosciences, University Bourgogne Franche-Comté, UMR CNRS 6282, France) was used for the acquisition of 3D images.

Author contributions

N.A., É.P.C., S.C. and K.M. designed the research; L.P., S.C., R.L. and K.M. organized the image analysis; N.A., L.P., R.L. and S.C. realized the images acquisition and reconstruction. N.A. wrote the paper, and all authors provided critical comments and were involved in the writing of the manuscript. All authors have read and agreed to the published version of the manuscript.

Competing interests

The authors declare no competing interests.

Additional information

Supplementary information The online version contains supplementary material available at <https://doi.org/10.1038/s41597-024-03641-1>.

Correspondence and requests for materials should be addressed to N.A. or K.M.

Reprints and permissions information is available at www.nature.com/reprints.

Publisher’s note Springer Nature remains neutral with regard to jurisdictional claims in published maps and institutional affiliations.



Open Access This article is licensed under a Creative Commons Attribution 4.0 International License, which permits use, sharing, adaptation, distribution and reproduction in any medium or format, as long as you give appropriate credit to the original author(s) and the source, provide a link to the Creative Commons licence, and indicate if changes were made. The images or other third party material in this article are included in the article's Creative Commons licence, unless indicated otherwise in a credit line to the material. If material is not included in the article's Creative Commons licence and your intended use is not permitted by statutory regulation or exceeds the permitted use, you will need to obtain permission directly from the copyright holder. To view a copy of this licence, visit <http://creativecommons.org/licenses/by/4.0/>.

© The Author(s) 2024